

Article

Parametric Process Design and Economic Analysis of Post-Combustion CO₂ Capture and Compression for Coal- and Natural Gas-Fired Power Plants

Emmanuel Adu ^{1,2}, Y.D. Zhang ^{1,3,*}, Dehua Liu ¹ and Paitoon Tontiwachwuthikul ⁴

¹ Department of Oil and Gas Storage and Transportation Engineering, School of Petroleum Engineering, Yangtze University, Wuhan 430100, China; adumax2000@yahoo.com (E.A.); DehuaLiu@126.com (D.L.)

² Mechanical Engineering Department, Faculty of Engineering and Technology, Kumasi Technical University, P. O. Box 854 Kumasi, Ghana

³ Measurement Science and Standards, National Research Council Canada, Building M-9, 1200 Montreal Road, Ottawa, ON K1A 0R6, Canada

⁴ Clean Energy Technologies Research Institute (CETRI), Faculty of Engineering and Applied Science, University of Regina, 3737 Wascana Parkway, Regina, SK S4S0A2, Canada; paitoon@uregina.ca

* Correspondence: zhangyindahust@yangteu.edu.cn

Received: 6 March 2020; Accepted: 6 May 2020; Published: 15 May 2020



Abstract: For the envisaged large number of commercial-scale carbon capture and storage (CCS) projects that are to be implemented in the near future, a number of issues still need to be resolved, the most prominent being the large capital and operational costs incurred for the CO₂ capture and compression process. An economic assessment of the capture and compression system based on optimal design data is important for CCS deployment. In this paper, the parametric process design approach is used to optimally design coal and natural gas monoethanolamine (MEA)-based post-combustion CO₂ absorption–desorption capture (PCC) and compression plants that can be integrated into large-scale 550 MW coal-fired and 555 MW natural gas combined cycle (NGCC) power plants, respectively, for capturing CO₂ from their flue gases. The study then comparatively assesses the energy performance and economic viabilities of both plants to ascertain their operational feasibilities and relative costs. The parametric processes are presented and discussed. The results indicate that, at 90% CO₂ capture efficiency, for the coal PCC plant, with 13.5 mol.% CO₂ in the inlet flue gas, at an optimum liquid/gas ratio of 2.87 kg/kg and CO₂ lean loading of 0.2082 mol CO₂/mol MEA, the CO₂ avoidance cost is about \$72/tCO₂, and, for the NGCC PCC plant, with 4.04 mol.% CO₂ in the inlet flue gas, at an optimum liquid/gas ratio of 0.98 kg/kg and CO₂ lean loading of 0.2307 mol CO₂/mol MEA, the CO₂ avoidance cost is about \$94/tCO₂.

Keywords: post-combustion; carbon capture and storage; coal-fired power plants; NGCC; energy; economic analysis

1. Introduction

The global increase in energy demand and the massive industrialization drive as a result of economic and demographic growth continue to increase the amount of greenhouse gas (GHG) emissions into the atmosphere. Emissions of greenhouse gases are responsible for climate change and global warming, with dangerous consequential impact on agriculture, water security, and sea level rise [1,2]. Carbon dioxide constitutes about 65% of the total anthropogenic GHG emissions [3,4]. Fossil fuels, coal, petroleum, and natural gas combustion processes are the main sources of CO₂ emissions [5,6], and they continue to dominate the global energy mix today, accounting for about 80% of the global primary energy demand [7,8], which needs to be decarbonized. Technology options that can deliver

the really deep decarbonation required in the power and industrial sectors may include the use of less carbon-rich fuels (such as a switch from coal to natural gas), as well as improvements in energy efficiency, renewable energy usage, carbon capture and storage (CCS), and nuclear-based energy generation [9–12]. The CCS technology is considered crucial and it is currently the only technology in the wider carbon emission mitigation approaches to achieve significant CO₂ emission reduction targets [13], with the post-combustion absorption–desorption capture (PCC) utilizing aqueous monoethanolamine (MEA) solvents being the most mature and industrial CO₂ capture technology commercially available currently [14].

In the power sector, currently, coal-fired power plants fuel 37% of global electricity, while natural gas-fired power plants fuel 24%, and oil power plants fuel 4% [8]. The installation of CCS on these power generation capacities is paramount. The International Energy Agency (IEA) projects that about 2500 large-scale CCS facilities should be in operation by mid-century [15]. However, globally, as of late 2019, there were only 19 large-scale CCS projects in operation, four under construction, 10 in advanced development using a dedicated front-end engineering design (FEED) approach, and 18 in early development, with these large-scale CCS plants either integrated into natural gas processing plants and/or power generation plants [16]. This means that more large-scale CCS plants are yet and will have to be built on most if not all fossil-based power plants before 2050. The challenge, however, is the high capital and operational cost of the CO₂ capture and compression process. According to Rubin et al. (2012), the capital and operational cost for capture and the compression process may account for close to 80% of the total CCS project costs [17]. Another challenge is that natural gas plants are being encouraged and are required to replace the high-emitting CO₂ coal-burning power plants as a CO₂ emission reduction measure; however, the capital and operational costs of the capture and compression process for natural gas plants remain high.

Current research areas of carbon capture and compression are the search for alternate solvents, as well as the use of flow scheme modifications to improve the capture process and heat integration between the carbon capture and compression process and the power plant; these approaches are all for the reduction of the capture process energy penalty, with an additional comparative analysis of carbon capture on coal and natural gas power plants. These research activities of carbon capture on coal- and/or natural gas-fired power plants were evaluated or studied at the pilot scale [18–22] and/or through process modeling [23–25] designs to provide the engineering data required for scale-up to large or commercial scale, since large-scale plants are expensive and much of these data are necessary for its actual implementation. Idem et al. (2006) compared the performance of MEA and mixed MEA/(methyldiethanolamine) MDEA solvents based on their heat requirement for solvent regeneration using two pilot CO₂ capture plants [18]. Notz et al. presented, in detail, information on the set-up and operation of a pilot plant based on an aqueous solution of MEA with sufficient data results that can be used for validation of models [19]. Frimpong et al. evaluated and compared the performance of an amine-carbonate blend with 30 wt.% MEA solvent under similar experimental conditions in a pilot plant [20]. Thompson et al. (a) and (b), in their studies, designed, constructed, and tested an advanced 0.7 MWe small pilot-scale post-combustion CO₂ capture system on a coal-fired power plant using a heat integration process combined with two-stage stripping. They assessed the solvent degradation products to determine the impact of oxygen exposure and also evaluated the overall amine, ammonia, and aldehyde emission levels from the solvent and degradation products [21,22]. In different process modeling studies of CO₂ capture, Berstad et al. reported a comparative study of natural gas combined cycle (NGCC)-, coal-, and biomass-fired power plants integrated with an MEA-based CO₂ capture plant and a compression system with a focus on energy performance for different desorber pressures [23]. Mac Dowell and Shah performed a study of the dynamic operations of a coal-fired power plant coupled with an MEA-based post-combustion CO₂ capture process [24]. Ali et al. investigated the comparative potential of different power generation systems, including natural gas combined cycle (NGCC) with and without exhaust gas recirculation (EGR), pulverized supercritical coal (PC), and biomass-fired power plants for constant heat input and constant fuel

flowrate cases when coupled with a CO₂ capture and compression system [25]. Since fossil-based power plants still remain the largest producers of CO₂ emissions and improvements in the CO₂ capture processes are needed for the best cost-saving options, the operational feasibilities of capturing CO₂ from these sources and the relative cost must be comprehensively evaluated.

Coal-fired and NGCC-fired power plants are considered in this study. The study discusses and uses the parametric process and design approach to optimally design coal and natural gas MEA-based PCC and compression plants that can be integrated into large-scale coal-fired and NGCC power plants, respectively. The study then comparatively assesses the energy performance and economic viabilities of both PCC and compression plants. The process design specification problems that this study sought to achieve were as follows: (a) what combination of the optimum liquid-to-gas molar flow rate ratio and column heights will combine with different process parameters to achieve the best process design for 90% capture rate with minimum electricity burden for the coal and NGCC capture plant solvent regeneration process and enhanced compression systems; (b) what will be the capital and operating cost of the process design plants in (a).

2. The Absorption-Desorption Process Modeling Approach

Process modeling of the absorption–desorption process for PCC processes was either developed on the assumption of equilibrium or rate-based mass transfer models. The equilibrium models, used to model absorption processes, may not predict such processes correctly, and rate-based models must be used [26,27]. The equilibrium model assumes that the vapor and liquid leaving the stage are in equilibrium. The mass transfer rate-based model assumes that there are gas and liquid films at the interface.

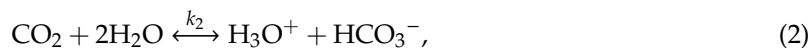
The process design experiment for sizing and evaluation of the process operating conditions was modeled using the electrolyte non-random two liquid (ENRTL) [28,29] model and the Peng–Robinson (PR) [30] model. The PR equation of state model was used for modeling the vapor phase non-ideal behavior, and the ENRTL activity coefficient model was used for rigorous modeling of the liquid electrolyte system (CO₂–MEA–H₂O systems). These models are based on extensive research and development in rate-based chemical absorption process simulation and molecular thermodynamic models for aqueous amine solutions [27]. They rigorously account for the vapor–liquid phase equilibrium, heat of absorption, and transport properties, as well as the chemistries of aqueous amine solutions.

The aqueous CO₂–MEA–H₂O system equilibrium reactions that occur during the cyclic absorption process and were incorporated into the models are as follows [31]:

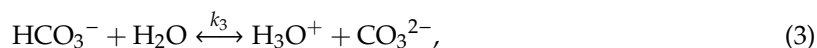
Water hydrolysis:



Bicarbonate formation:



Dissociation of bicarbonate:



Dissociation of protonated amine:



Dissociation of protonated carbamate:



where k_i represents the reaction kinetic rate constants.

The mass and heat transfer processes of the absorption–desorption process take place between the gas and liquid phases throughout the stages in the column. For gas–liquid reacting systems, both physical mass transfer and chemical reactions occur. The rate of mass transfer in an absorption process of CO_2 in a given solvent will involve the diffusivity of CO_2 through the solvent, solubility of CO_2 in the solvent, and the chemical reactivity between CO_2 and the base present in the solvent. Figure 1 shows a schematic diagram of the CO_2 transport during an absorption process.

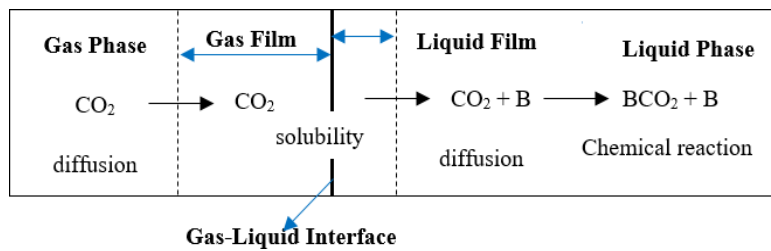


Figure 1. Rate-based CO_2 absorption process from the gas phase to the base (B) present in liquid solvent.

The absorption mechanism involves CO_2 diffusing through the gas phase and then dissolved (soluble) within the gas–liquid interface. The liquid phase is the limiting aspect of the rate of mass transfer of CO_2 through the interface, and the CO_2 reaction will only occur beyond the gas–liquid interface in the liquid solution phase. For the desorption process, the CO_2 is disengaged from the liquid phase into the gaseous phase. The rate of mass transfer of CO_2 (the change in the concentration of CO_2 per time) in the gas–liquid interface is given as follows [32]:

$$\frac{dC_{\text{CO}_2}}{dt} = K_{L,\text{CO}_2}(C_{i,\text{CO}_2} - C_{\infty,\text{CO}_2}), \quad (6)$$

where K_{L,CO_2} is the mass transfer coefficient of CO_2 at the liquid phase, and C_{i,CO_2} and C_{∞,CO_2} are the concentrations of CO_2 at the gas–liquid interface and within the solution fluid, respectively. For amine solutions, Henry’s partitioning from amine solutions is very different than from pure water. For CO_2 -alkanolamine– H_2O systems, the solubility (concentration) of CO_2 at the interface is determined using Henry’s law as given below.

$$P_{\text{CO}_2,g,i} = H_{\text{CO}_2} \times [\text{CO}_2]_i, \quad (7)$$

where $P_{\text{CO}_2,g,i}$ is the partial pressure of CO_2 in the gas phase at the interface, H_{CO_2} is Henry’s law constant of CO_2 , and $[\text{CO}_2]_i$ is the concentration of dissolved CO_2 at the interface.

The absorption process of CO_2 into aqueous amine solution involves CO_2 diffusion and a chemical reaction within the liquid phase between the solution-phase CO_2 and a reactive base component present in the liquid solvent solution, forming a carbamate (C–N) or carbonate (C–O) bond. The CO_2 crosses the gas–liquid interface and it is assumed to react quickly with the base in the reaction process to form products; hence, the CO_2 concentration in the solution fluid (C_{∞,CO_2}) is approximately zero. The rate of chemical absorption/desorption of CO_2 in the liquid-phase solution is given as follows [32]:

$$\frac{dC_{\text{CO}_2}}{dt} = C_{i,\text{CO}_2} \times K_{L,\text{CO}_2} \times E, \quad (8)$$

where E is the enhancement factor, associated with the enhancement of the rate of absorption based upon the chemical reaction in the solution, and it can be calculated as follows:

$$E = \frac{\sqrt{M\left(\frac{E_i - E}{E_i - 1}\right)}}{\tanh \sqrt{M\left(\frac{E_i - E}{E_i - 1}\right)}}, \quad (9)$$

such that

$$\sqrt{M} = \frac{\sqrt{D_{L,CO_2} K_2 C_B}}{K_{L,CO_2}}, \quad (10)$$

and

$$E_i = \left(1 + \frac{D_B C_B}{z D_{L,CO_2} C_{i,CO_2}}\right), \quad (11)$$

where E_i is the instantaneous reaction enhancement factor, D_{L,CO_2} is the CO_2 diffusivity in the liquid phase, E_2 is the rate constant, C_B is the concentration of the reactive base component in solution, D_B is the diffusivity of the reactive base component, and z is the stoichiometric coefficient of the reactive base component.

3. Project Specifications and PCC and Compression Unit Operations

3.1. Project Specifications

In order to design an industrial-scale optimum solvent-based post-combustion CO_2 capture plant, two specific power plants, namely, a 550 MWe pulverized supercritical coal-fired (coal) power plant with a flue gas CO_2 concentration of 13.5 mol.% and a 555 MWe natural gas combined cycle (NGCC) power plant with a flue gas CO_2 concentration of 4.04 mol.%, were chosen. The flue gas conditions and compositions for both power plants were obtained from a 2013 report by the United States (US) Department of Energy/National Energy Technology Laboratory (USDOE/NETL) [33]. The power plant specifications and conditions and the compositions of both flue gases are shown in Table 1.

Table 1. Power plant specifications and flue gas conditions [33].

Parameter	Unit	Coal	NGCC
Fuel type		Coal	Natural gas
Net power output	MWe	550	555
LHV/HHV (MWth)	LHV/HHV	HHV (1400)	HHV (1106)
Power plant efficiency	%	39.3	50.2
Flue gas properties from power plant			
Temperature	K	331.15	379.15
Pressure	MPa, abs.	0.10	0.10
Mass flow rate	kg/s	821.26	897.4
Composition			
N_2	mol.%	67.93	74.32
O_2	mol.%	2.38	12.09
CO_2	mol.%	13.5	4.04
H_2O	mol.%	15.37	8.67
SO_2	ppm	0	0
NO_x	ppm	N/A	0
H_2S	ppm	N/A	0
Ar	mol.%	0.81	0.89

HHV: Higher Heating Value; LHV: Lower Heating Value; NGCC: Natural Gas Combined Cycle; N/A: Not Applicable.

3.2. Base Flowsheet Unit Operations of the Amine PCC and Compression System

The typical amine-based post-combustion CO₂ capture and compression process flowsheet consists mainly of an absorber unit, water wash section, regeneration unit with a reboiler and a condenser, lean/rich amine heat exchanger, water and amine makeup, amine cooler, and rich and lean amine pumps. Figure 2 shows the standard process flow diagram of CO₂ capture with a compression system.

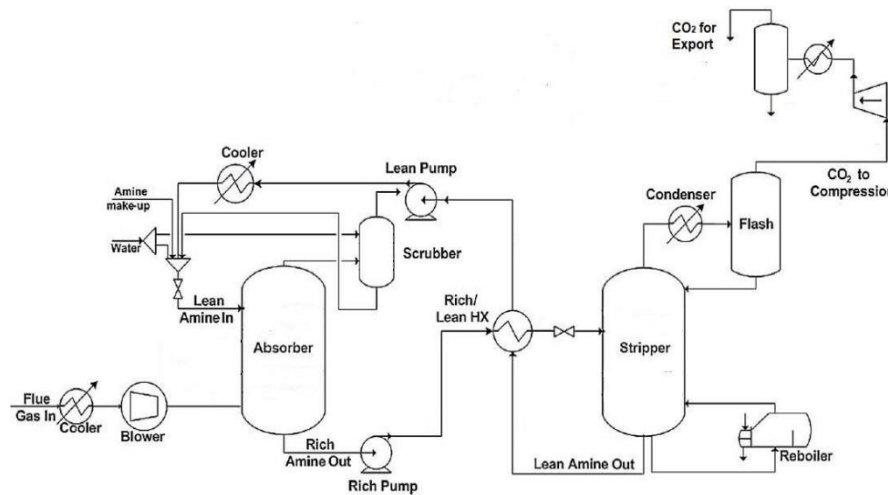


Figure 2. Standard process flow diagram of CO₂ capture with a compression system.

The power plant combustion flue gas temperature ranges from approximately 650 °C at the boiler or heat recovery steam generator (HRSG) exit down to approximately 40–65 °C at the stack. A direct-contact cooler (DCC) system initially quenches and lowers the temperature and saturates the incoming flue gas using counter-current flow water in order to improve the efficiency of the absorption process and provide pre-scrubbing on the flue gas. The cooled flue gas containing CO₂ is moved by a fan or blower and enters the absorber at the bottom, while the lean amine solution is pumped into the top of the absorber. The movement of the flue gas by the fan or blower helps overcome the pressure drop between the power plant and absorption column. A water wash section is located in the upper region of the absorber to scrub and clean the flue particularly of any solvent carry over in the CO₂ depleted flue gas, as well as to maintain the water balance of the lean solution system into the absorber by adjusting the temperature of the circulating water of the upper water-wash section. In the absorber unit, the CO₂ gas mixture moves up and the amine solution moves down the absorption tower, which has packing material in it that enhances the interactions of gas-to-liquid contact. As the amine solution moves down the stages, it gains CO₂ and becomes rich in CO₂. The CO₂-rich amine is then pumped through the lean/rich amine heat exchanger where it is heated before entering the stripper or regenerator column. The stripper is modeled as a distillation column. In the stripper unit, the amine solution which is rich in CO₂ flows down the stripper through the packed bed counter-current before flowing up stripping steam which strips off the CO₂ gas from the rich solvent, and the solvent is regenerated as a lean amine solution at the bottom of the stripper. The entire solution in the stripper unit, which has about 70 wt.% water, is heated up by the reboiler heater (heat input provided by a condensing low-pressure (LP) steam typically from the power plant) to form steam, used to break the bonding interaction between the CO₂ and the amine in that solution for the stripping process. The heated regenerated lean amine solution is then pumped through the lean/rich amine heat exchanger to heat up the CO₂-rich amine from the absorber exit, in order to increase the CO₂ partial pressure in the solution for easy stripping. The lean amine solution from the stripper is combined with water and amine as makeup streams at the same pressure in a makeup operation before passing through the amine cooler and then being recycled back into the absorption unit. An overhead vapor from the top of the stripper containing CO₂ saturated with water is partially condensed by the stripper condenser,

and part or all the condensed liquid water is returned back into the reflux drum to be pumped to the stripper as a reflux. The process is a continuous one by continuously regenerating the lean amine solution in the stripper unit and sending it back to the absorber unit, whilst the overhead CO₂-rich vapor is generated at the top of the stripper.

The overhead CO₂-rich vapor is then conditioned by a water condenser and separator and sent to the CO₂ product compressor for compression and pipeline transport. A multiple-stage compression process is used for controlling the discharge temperature and limiting pressure drops with CO₂ gas stream cooling performed in between, downstream of each compression stage, followed by dehydration in knock-out drums.

4. Results and Discussion

4.1. Validation of Model

The experimental data of absorption (solubility) of CO₂ in aqueous solutions of MEA from Sheng and Li (1992) [34] and the pilot plant data of the specific reboiler duty reported by Notz et al. were compared with the model data results for purposes of validating the model's accuracy. For the solubility data from Shen and Li, the temperature and pressures were targeted, while, for the specific reboiler duty data from Notz et al., the lean loading was targeted during the model validation. Table 2 shows the experimental and model results. Average absolute relative deviation (AARD) values of 2.6% for the solubility and 5.2% for the specific reboiler duty were obtained, thus indicating a very good representation of experimental data.

Table 2. Simulation and experimental data comparison.

Solubility of CO ₂ in 30 wt.% Aqueous Solution of MEA [34]				Specific Reboiler Duty in kJ/kgCO ₂ [19]		
T (°C)	P (kPa)	Mol CO ₂ /mol MEA (Experiment)	Mol CO ₂ /mol MEA (Model)	Lean Loading Mol CO ₂ /mol MEA	GJ/tCO ₂ Experiment	GJ/tCO ₂ Model
40	28.7	0.538	0.563	0.265	5.01	5.412
40	58.4	0.570	0.615	0.308	3.98	3.628
40	101.3	0.594	0.625	0.230	7.18	7.345
60	61.0	0.526	0.543	0.268	5.05	5.216
60	96.5	0.557	0.576	0.306	4.19	4.015
60	116.3	0.567	0.586	0.317	3.85	3.675

The objective function (% AARD) used in this paper between the model predictions and the experimental data is defined as follows:

$$\text{Objective function}(\%AARD) = \frac{1}{N} \sum_{j=1}^N \frac{|\text{CO}_2^{\text{Exp}} - \text{CO}_2^{\text{Model}}|}{\text{CO}_2^{\text{Exp}}} \times 100, \quad (12)$$

where N is the number of experimental data points, CO_2^{Exp} is the experimental CO₂ data value, and $\text{CO}_2^{\text{Model}}$ is the predicted model data value.

4.2. Parametric Process Design Analysis Results

In this study, the parametric analysis approach was adopted to size the PCC and compression equipment and to evaluate the process operating conditions for both the 550 MWe Coal and the 555 MWe NGCC power plant capture units. The CO₂ capture efficiency and solvent regeneration

thermal energy demand, as well as other key factors of the absorption process, are discussed. The CO₂ capture efficiency of the PCC facility in this paper is defined as follows:

$$\text{CO}_2 \text{ Capture Efficiency} = \frac{\text{CO}_{2in} - \text{CO}_{2out}}{\text{CO}_{2in}} \times 100, \quad (13)$$

where CO_{2in} is the CO₂ flow in the flue gas entering the absorber and CO_{2out} is the CO₂ flow exiting the absorber in the depleted or treated gas.

The solvent absorbent regeneration energy is calculated as follows [35,36]:

$$\text{Re generation Energy} = \frac{H_{reboiler}}{m_{\text{CO}_2}} = Q_{sens} + Q_{\text{CO}_2} + Q_{\text{Vap,H}_2\text{O}}, \quad (14)$$

where $H_{reboiler}$ is the reboiler heat duty, m_{CO_2} is the mass flow rate of CO₂ produced, Q_{sens} is the sensible heat requirement, Q_{CO_2} is the energy required for CO₂ desorption, and $Q_{\text{Vap,H}_2\text{O}}$ is the steam or water evaporation energy.

Specifically, results of the effect of the absorber and stripper column packed height, solvent concentration and CO₂ solvent lean loading, absorber lean solvent temperature, stripper reboiler temperature, CO₂-rich loading, stripper inlet temperature, and stripper inlet pressure on the design of the absorption–desorption process requirement for the specified power plant flue gas are presented in the subsequent subsections.

Qualitatively, the trends of the parametric analysis studies are very similar for both studied power plant unit's flue gases. Thus, only the results of the coal-fired power plant are shown here. The final improved performance results of the capture equipment for both plants are, however, presented under Section 4.3. Figures 3 and 4 shows the base case flowsheet diagram of the amine-based post-combustion CO₂ absorption-desorption capture process and the compression system model used in this paper.

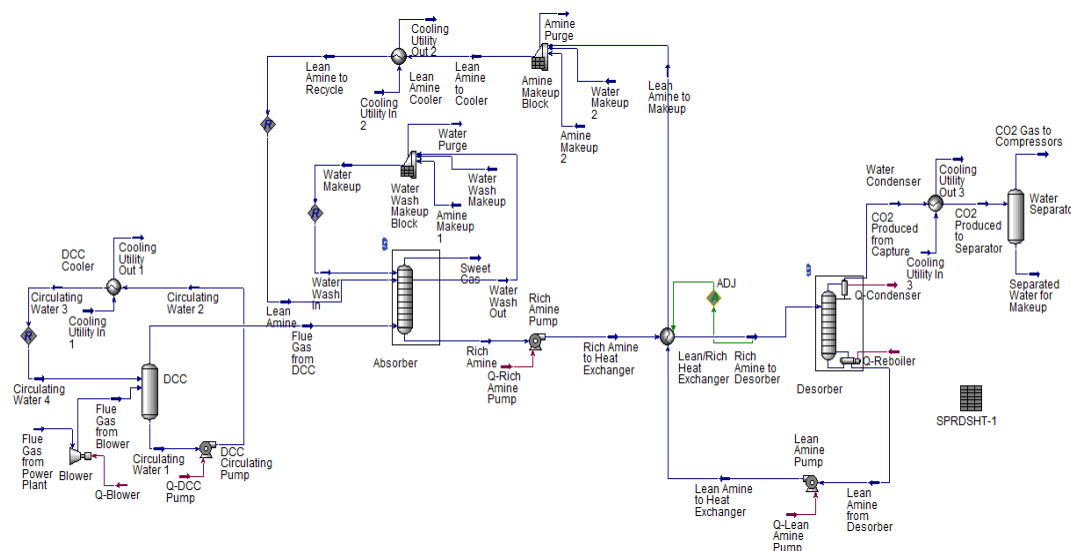


Figure 3. Base flowsheet of amine-based post-combustion CO₂ absorption–desorption capture process.

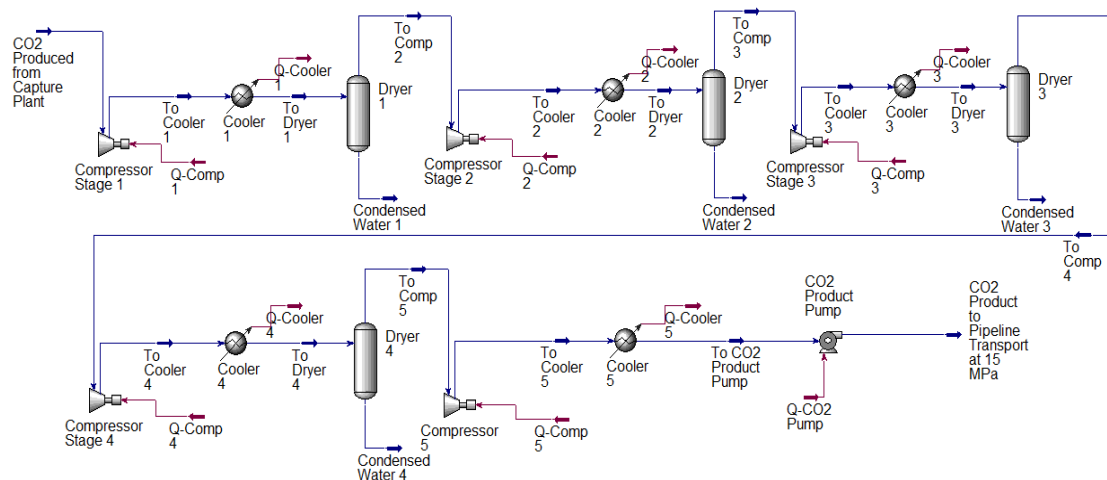


Figure 4. Flow diagram of the CO₂ compression system model. The captured CO₂ product stream is compressed in five intercooled stages and subsequently pumped to a pipeline transport pressure of 15 MPa.

4.2.1. Effect of Absorber and Stripper Column Packed Height

For an absorption and stripping column process design, the recovery percentage of the solute CO₂ in the gas mixture and the required product purity of separation are largely determined by the liquid-to-gas molar flow rate (L/G) ratio and the packed height of the absorber or stripper columns. However, there is always a trade-off between the liquid-to-gas molar flow rate ratio and the packed height required. The optimal solvent rate for an absorption/desorption process is determined by balancing the operating costs of the absorber and stripper with the fixed capital equipment costs. Figure 5 shows the effect of the L/G ratio on the CO₂ capture efficiency and the regeneration energy for an absorber with packed heights of 40, 41, and 42 m. The stripper was modeled with a packed height of 18 m and a base case MEA concentration of 30 wt.%. The typical solution strength of MEA ranged from 10 wt.% to 30 wt.%, with 30 wt.% considered as an industry benchmark. Moreover, increasing the MEA concentration above 30 wt.% leads to plant corrosion tendencies [37,38].

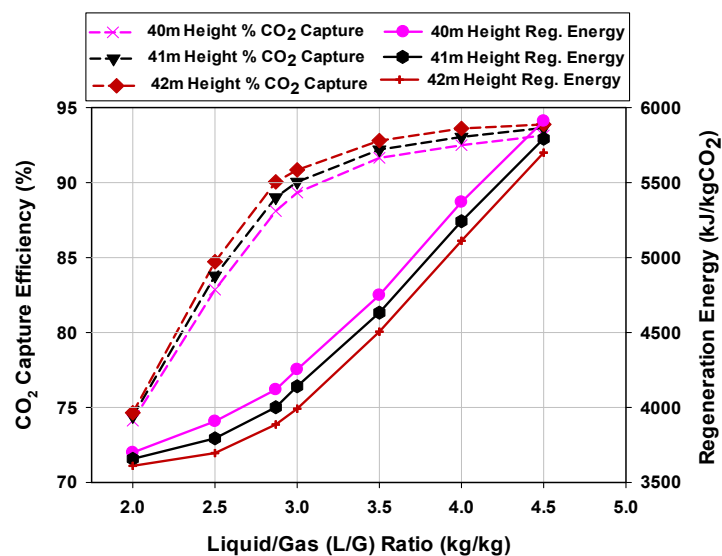


Figure 5. Effect of the liquid-to-gas (L/G) ratio on the CO₂ capture efficiency and the regeneration energy for different absorber column packed heights.

The lean MEA solution flowrate exiting the bottom of the stripper and entering the top of the absorber was varied between 1706 and 3839 kg/s. Figure 5 shows that a lower solution flowrate resulted

in a lower amount of CO₂ that could be absorbed. At these lower values, the vaporization of water required for CO₂ stripping contributed most to the regeneration energy. At an L/G ratio of about 2.87 (lean flowrate of 2451 kg/s), the CO₂ capture efficiency was equal to or greater than 90 M% for the absorber column packed height of 42 m. The 40-m and 41-m heights achieved 90% capture rate at higher L/G values. A higher column packed height implies high capital cost. However, at the L/G ratio of 2.87, the 42 m height absorption process had the minimum regeneration energy of 3886 kJ/kg CO₂ compared to the 40 m and 41 m heights with regeneration energies of 4119 and 4001 kJ/kg CO₂, respectively. On this basis, an optimum solvent flow rate of 2451 kg/s and an absorber column with a packed height of 42 m were selected with minimum regeneration energy demand.

For CO₂ capture from flue gases using an amine absorption-stripping system, the use of a shortcut method model (Fenske-Underwood-Gilliland model) [39–41] in simulations to determine the required stripper stages and, hence, the optimal design of the stripper system may not be feasible because of the low mole fraction of CO₂ produced as the light key component and the temperature limitations of the system. Therefore, stage-by-stage approach calculations were used. The effect of the stripper reboiler and condenser heat duty on the CO₂ capture percentage for different stripper column packed heights is illustrated in Figure 6. The heating supply to the stripper reboiler was provided by condensing low-pressure (LP) steam typically generated from the power plant. This maximizes the exergy in the integration process system. A full reflux condenser system was used, and the condenser temperature was set to 90 °C. This temperature impacted the amount of water produced with the overhead gaseous CO₂ product generated at the top of the stripper for compression and the condensed liquid returning to the stripper, which should be kept high to enhance regeneration efficiency in the stripper. The reboiler temperature was set to 117 °C to ensure little or no MEA degradation [42]. Figure 6 shows an increase in the reboiler and condenser duty with increasing CO₂ capture percentage for the stripper column with packed heights of 16, 17, and 18 m.

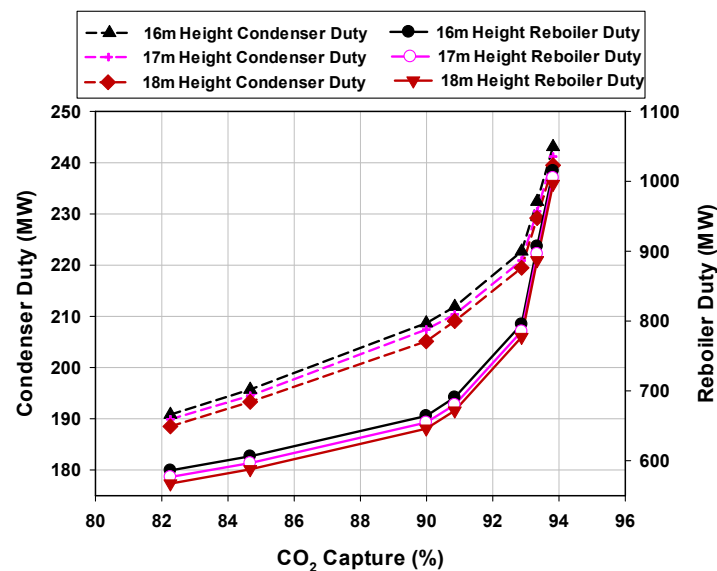


Figure 6. Effect of the stripper reboiler and condenser heat duty on the CO₂ capture percentage for different stripper column packed heights.

The increase in CO₂ capture leading to an increase in reboiler and condenser duty was a result of the increase in the lean amine solution molar flow rate. Increasing the solution flow or capture rate requires a proportionate increase in heat supply for CO₂ desorption from the rich solution since the absorbed mass of CO₂ increases in the rich solution, an increase in heat supply to raise the solvent temperature to that of the reboiler, and an increase in heat supply for steam generation (water evaporation) by the reboiler heater for processing the increasing solution amount. The increase in the total reboiler heat duty enhanced the regeneration efficiency in the stripper. These processes also

resulted in higher condenser heat duty requirement. The figure indicates a much lower condenser and reboiler heat duty for the stripper with 18 m height. At a reboiler duty of 645 MW and a condenser duty of 205 MW, the CO₂ capture was 90 M% or more for the stripper with 18 m packed column height.

4.2.2. Effect of MEA Solvent Concentration and Lean Loading

The effect of the MEA concentration on the CO₂ capture efficiency and the regeneration energy is shown in Figure 7. The figure indicates that increasing the MEA concentration from 15 wt.% to 40 wt.% increased the capture rate by close to 40%. This phenomenon can be attributed to the increased CO₂-loading capacity of the MEA solvent as the concentration was increased, leading to higher absorption rate. At these higher absorption rates, the required working rate of the solvent flow was reduced, which resulted in the reduction of the regeneration energy. A higher concentration of the amine in the solution means that more CO₂ can be absorbed and desorbed by the same solvent flowrate. Hence, the regeneration energy requirement is lower.

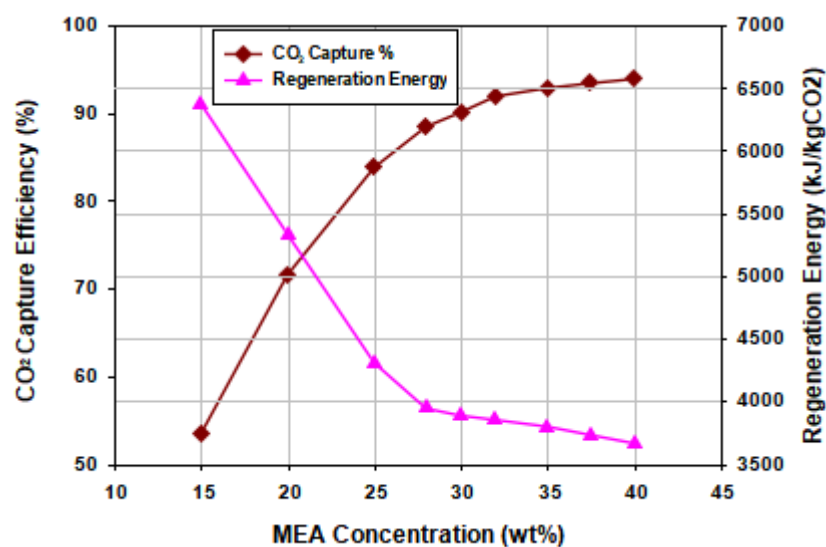


Figure 7. Effect of the MEA concentration on the CO₂ capture efficiency and the regeneration energy.

As confirmed by Figure 7, it is observed that, at an MEA concentration of 30 wt.% and above, 90% capture or more was achieved with lower regeneration energy. In order to compare the efficiency of the regeneration for increasing the MEA concentration, regeneration efficiency is defined here as the ratio (percentage) of the difference between the amount of protonated rich amine and lean amine loadings to the protonated rich amine loading. The regeneration efficiencies of 30 wt.%, 32 wt.%, 35 wt.%, 37.5 wt.%, and 40 wt.% in the stripper were studied at the same solvent flowrate (2451 kg/s) and operating conditions of the absorption-stripping process in order to comparatively assess their performance.

Figure 8 shows that the improvements in the regeneration energy of the stripper performance by increasing the amine concentration in the solution were limited, particularly above the set design capture rate of 90%. The regeneration efficiency decreased with increasing MEA concentration. Whereas the 30 wt.% MEA solution achieved a regeneration efficiency of 60% of its amine content, the 32 wt.%, 35 wt.%, 37.5 wt.%, and 40 wt.% MEA solutions achieved lower regeneration efficiencies of 56%, 51%, 47%, and 43%, respectively. High MEA concentrations led to higher amine loss. This result also indicates that improvements in the efficiency of the desorption-regeneration process should be of equal importance in order to decrease the cost of CO₂ capture instead of the current focus on the capture efficiency above the 90% capture rate. Moreover, increasing the MEA concentration above 30 wt.% leads to plant corrosion tendencies [37,38].

From Figure 7, the optimum MEA concentration of 30 wt.% corresponding to a 90% capture efficiency resulted in a regeneration energy of 3886 kJ/kg CO₂.

The lean CO₂ loading impacts the loading capacity of the MEA absorption process. The difference between rich CO₂ loading of the solvent at the bottom of the absorber and the lean CO₂ loading at the bottom of the stripper, known as the cyclic capacity, is an important measure of the PCC plant process design. Higher cyclic capacity means a larger amount of CO₂ captured by a specified amount of the solvent. Utilizing the optimum 30 wt.% MEA solution, 90% CO₂ capture capacity was set at different lean loadings. This was achieved by tweaking the lean solvent flow rate and the reboiler energy input. Figure 9 shows the variations in the lean solvent flow rate and the obtained regeneration energies. It indicates that the selected lean loading can be used to minimize the solvent regeneration energy requirement at a specified solvent flow rate.

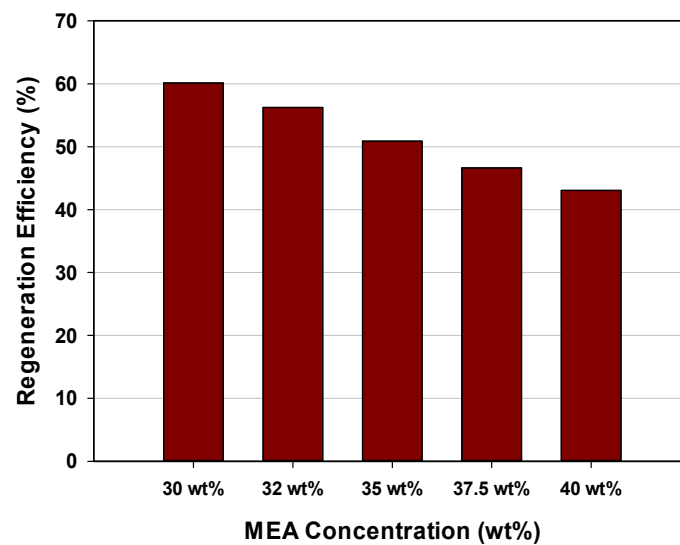


Figure 8. Effect of MEA concentration on the regeneration efficiency of the absorption–stripping system (at a solvent rate of 2451 kg/s).

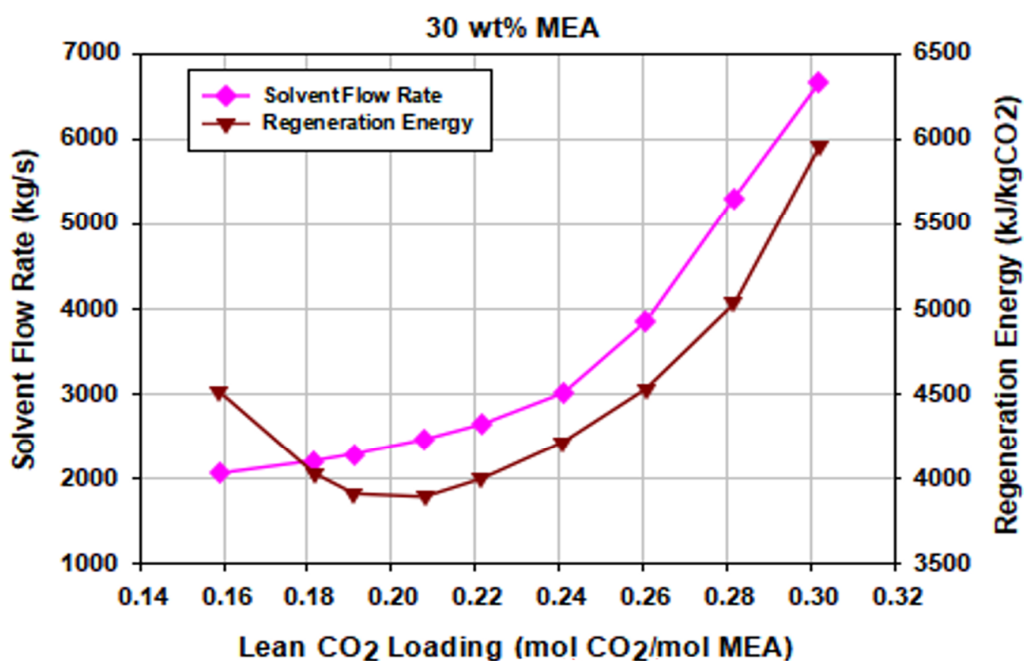


Figure 9. Effect of solvent lean loading on the solvent flow rate (90% CO₂ capture) and regeneration energy of the stripper.

The figure shows that the regeneration energy decreased with increasing lean loading until a minimum was achieved. This is consistent with observations by previous works [43–45]. This phenomenon is due to the fact that lower solvent flowrates are required at the lower lean loadings to maintain a 90% constant capture rate before reaching the minimum energy point. With a low solvent flowrate, the residence time of the solution in the stripper becomes longer and more stripping steam than actually necessary is generated in the reboiler, resulting in high energy duty at lower lean solvent loadings. Lower lean loadings, however, enhance the rate behavior of the absorber.

At higher values of lean loadings (above the optimum lean loading), additional energy is required in the form of sensible heat for heating solvent due to the increased amount of solvent required to maintain a constant capture rate. Hence, there is a pronounced energy minimum which occurs at the optimum lean loading. The optimum lean loading reached at the optimal solvent flow rate corresponding to the minimum energy required to regenerate the solvent in the stripper is about 0.2082 mol CO₂/mol MEA.

4.2.3. Effect of Absorber Inlet Lean Solvent Temperature and Water Wash System Temperature

The temperature of the lean solvent entering the top of the absorber was varied between 25 and 60 °C for the 42-m-height absorber and 18-m-height stripper. Figure 10 shows a slight decrease in the CO₂ capture efficiency upon increasing the lean solvent temperature. This is due to the fact that an increase in temperature of the lean solvent decreased the solubility (driving force for CO₂ transfer from the gas phase into the liquid phase) of the absorbent, thus reducing the separating efficiency of the absorption process. However, this slight decrease kept the CO₂ capture rate close to 90 %.

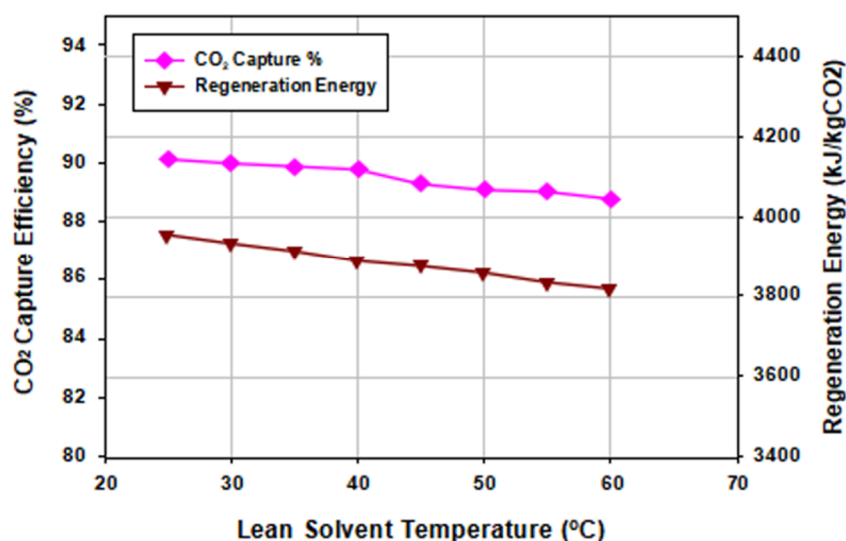


Figure 10. Effect of lean solvent temperature on the CO₂ capture efficiency and the regeneration energy.

Increasing the lean solvent temperature caused a slight decrease in the regeneration energy. This slight decrease was due to the small decrease in the flowrate of the rich solution which exited the bottom of the absorber as the lean solvent temperature increased, and which then entered the stripper. This decreasing effect of the flow rate of the rich MEA solution at the stripper inlet requires less sensible heating and, hence, a reduction in the regeneration energy. However, at higher operating temperatures, the evaporation rate of MEA was high.

For an absorption–stripping process, the water wash system located in the upper region of the absorption tower was used to maintain the water balance of the lean solution system into the absorber by adjusting the temperature of the circulating water of the upper water wash section. Higher lean solvent temperatures resulted in higher-temperature operating conditions of the water wash section (in this study, temperature of the water wash system increased by 14 °C, i.e., from 57 to 71 °C when

the lean solvent temperature was varied between 25 and 60 °C) and, hence, higher cost. Therefore, the optimal lean solvent temperature was selected to be that which met the design capture rate, gave a relatively low regeneration energy, and still maintained fairly reasonable and favorable temperature operating conditions of the water wash system.

4.2.4. Effect of Stripper Reboiler Temperature

As mentioned previously, the reboiler energy input was provided using a condensing low-pressure (LP) steam typically generated from the power plant. This energy requirement can also be supplied from other heat sources such as an electrical heating element. The experimental lab-scale stripper design utilized a reboiler temperature controlled from heating oil in a thermostat. The reboiler temperature was varied between 116 and 120 °C. Figure 11 shows that both the capture efficiency and regeneration energy increased with reboiler temperature.

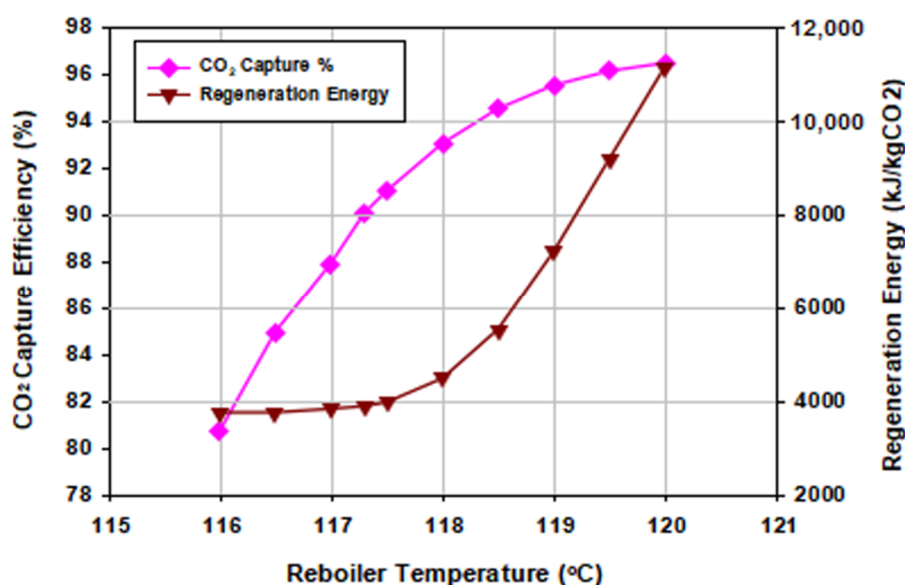


Figure 11. Effect of reboiler temperature on the CO₂ capture efficiency and the regeneration energy.

At lower temperatures, less energy was required by the reboiler; hence, the amount of steam was in less demand but was still needed for the stripping of the captured CO₂ in the rich solution. At these lower temperatures, the desorption–regeneration efficiencies were low with higher lean loadings (at 116 °C achieved lean loading was 0.26 mol CO₂/mol MEA), which led to poor absorption capacities. On the other hand, by increasing the reboiler temperature a higher amount of stripping steam was generated in the reboiler with rather higher desorption–regeneration efficiencies and lower lean loadings (at 120 °C, the achieved lean loading was 0.1 mol CO₂/mol MEA). Thus, the optimal operating stripper reboiler temperature was selected to be that with a relatively low regeneration energy which still maintained a reasonable desorption–regeneration efficiency.

4.2.5. Effect of Rich Loading

The CO₂ loading of the rich amine solution, which depends on the operating conditions of the absorption–stripping process, significantly impacts the reboiler energy requirements. A high heat of absorption in the absorber is required for the MEA reaction with CO₂ to form a carbamate and a protonated amine, which limits the theoretical rich loading to a maximum of around 0.5 mol CO₂/mol MEA [46]. At loadings higher than this theoretical value, bicarbonates are formed as part of the solution. The differences in the CO₂-loaded rich amine solution entering the stripper imposed changes in the reboiler energy demand. As can be seen in Figure 12, stripping CO₂ from lower rich loadings required high regeneration energy of the reboiler. This was due to the fact that, at lower rich loadings,

the vapor–liquid equilibrium conditions shifted with a reduction in the CO₂ partial pressure, and the presence of a carbamate (C–N) bond is prominent. This resulted in increase in the amount stripping steam for the release of CO₂.

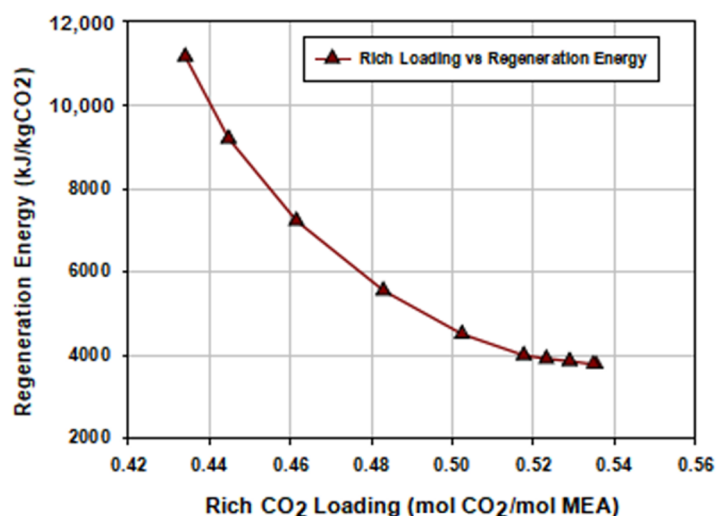


Figure 12. Effect of the rich CO₂ loading on the regeneration energy of the reboiler.

As the rich loading increased, the formation of a relatively weak unstable bicarbonates occurred and the reboiler energy demand decreased, with a decrease in the amount of steam required for desorption of CO₂. More unstable bicarbonates became apparent in the solution over the maximum loading value and, therefore, lower but small changes in reboiler energy were required for desorption–regeneration, as depicted in Figure 12, after the 0.5 mol CO₂/mol MEA. The regeneration energy reached its lowest point (3755 kJ/kg CO₂) at a rich CO₂ solvent loading of around 0.536 mol CO₂/mol MEA. The figure also indicates that an increase in the rich loading from 0.45 to 0.5 mol CO₂/mol MEA led to a reduction in the reboiler energy demand of about 50%. Consequently, an MEA CO₂ absorption operation that achieved a rich loading close to 0.5 mol CO₂/mol MEA was optimal.

4.2.6. Effect of Stripper Inlet Temperature and Pressure

The rich amine solution was preheated by the lean/rich amine heat exchanger before entering the stripper. The temperature at which the rich amine solution leaves the heat exchanger also determines the CO₂ partial pressure of the solution and, hence, the entire operational performance of the stripper column and reboiler duties. An increase in the temperature of the rich solution increases the CO₂ partial pressure in the solution and, at a high rich CO₂ loading, enhances the stripper and reboiler performance to some extent, increasing the driving force for the CO₂ desorption–amine regeneration process. The effect of varying the stripper inlet temperature and pressure conditions at rich loadings of 0.5 mol CO₂/mol MEA on the regeneration energy, keeping all other operating conditions constant, is shown in Figure 13.

Figure 13 indicates that an increase in the rich amine inlet temperature and, thus, the inlet pressure decreased the regeneration energy requirement of the stripper. An increase from 96 °C (150 kPa) to 120 °C (240 kPa) led to about 10% reduction in the stripper regeneration energy. This was due to the lower temperature difference between the stripper top inlet and the reboiler. Increasing the feed temperature from 96 to 120 °C only saw a small change in the lean loading, from 0.2 to 0.21 mol CO₂/mol MEA. This indicates that increasing the inlet temperature had little effect on the amine regeneration efficiency. Due to amine degradation and corrosion at high temperatures, the optimal stripper inlet temperature and, thus, the pressure was chosen not to be too high, at least within a 10 °C temperature difference lower than the reboiler temperature.

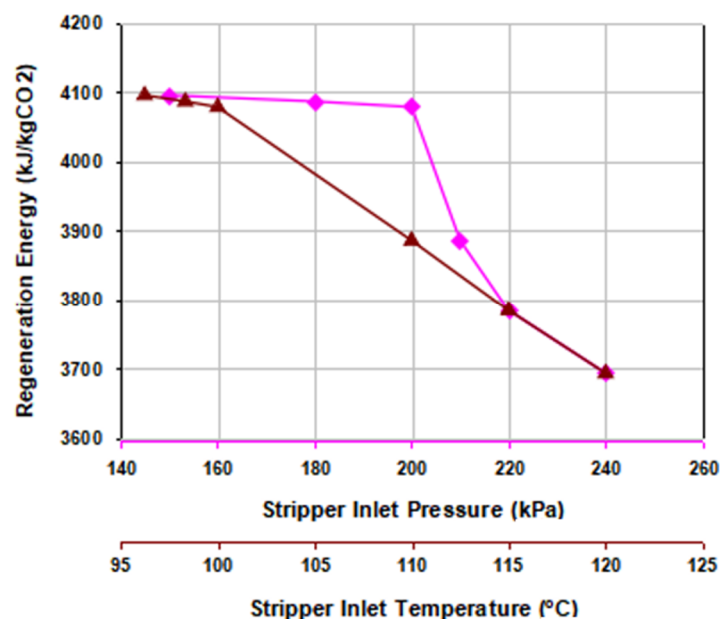


Figure 13. Effect of different stripper inlet temperatures and pressures at rich loadings of 0.5 mol CO₂/mol MEA on the regeneration energy.

4.3. Summary of Optimized Process Design and Operating Conditions of PCC and Compression with Coal and NGCC Power Plants

The improved process design of the PCC and compression system integrated with both coal and natural gas power plants incorporates almost all process equipment that is required in a full-scale CO₂ capture plant and a compression system. These include the blower, direct contact cooler (DCC), absorber, water wash section, rich and lean amine pumps, lean/rich heat exchanger, stripper with a condenser and reboiler, water and amine makeup block, lean amine cooler, water condenser and separator, and a five-stage CO₂ compression with intercooling and drying systems.

The improved design and operating condition results of the PCC and compression units, obtained via comprehensive simulations, are presented in the subsections below.

4.3.1. Improved Results for PCC and Compression with Coal-Fired Power Plant

The improved PCC and compression facility integrated with the coal-fired power plant was designed to capture 90% of the CO₂ in the flue gas (FG) from the flue gas desulfurization (FGD) unit of the power plant. The FG blower was installed upstream the coal power plant DCC to facilitate the effective cooling of the FG before entering the absorber tower. The FG blower operated at an inlet pressure and temperature of 100 kPa and 58 °C, respectively, and an outlet pressure and temperature of 110 kPa and 69.4 °C, respectively, i.e., the FG pressure was boosted in the FG blower by 10 kPa to overcome the pressure drop in the CO₂ absorber column, resulting in a blower power duty of 10.1 MW. The DCC cooled and conditioned the FG pressure, temperature, and moisture content so it met the requirement of the absorption column. The temperature and, hence, moisture content of the FG exiting the FGD was reduced in the DCC, where the FG was cooled using cooling water condensed from the FG and recirculated to the top of the DCC. This slightly affected the condition and compositional amount of the FG that existed the DCC and entered the absorber, and it resulted in a pressure of 110 kPa, temperature of 40.02 °C, and FG flowrate of 853.1 kg/s.

For the absorption–stripping process, a lean solvent temperature of 40 °C at a pressure of 101.3 kPa and stripper inlet temperature of 110 °C at a pressure of 210 kPa were selected. An optimum solvent flow rate of 2451 kg/s, MEA concentration of 30 wt.%, absorber column with Mellapak 250Y packings with a total packed height of 41.50 m, rich CO₂ loading of 0.5226 mol CO₂/mol MEA, stripper column with Mellapak 250Y packings with a total packed height of 18 m, and reboiler temperature of 117.3 °C

were obtained with a minimum regeneration energy of 3886 kJ/kgCO₂ at a lean CO₂ loading of 0.2082 mol CO₂/mol MEA.

Optimal parameters of the other ancillary process equipment obtained were as follows: lean/rich heat exchanger duty, 503.9 MW; lean amine cooler duty, 143.9 MW; lean amine pump duty, 400.4 kW; rich amine pump duty, 585.8 kW; water wash section operating temperature, 65 °C; water condenser duty, 270.1 MW; and total cooling water requirement of the coal capture plant, 16320 kg/s.

The overhead CO₂ product stream exited from the stripper top at a pressure of 120 kPa, temperature of 91 °C, and CO₂ mass flow of about 600 tons per hour, corresponding to a mass purity of about 97 %. The CO₂ product stream was cooled down to 40 °C in the water condenser, and water was separated from the stream in the water separator. The cooled stream was sent to the five-stage compression system composed of a series of compressors, intercoolers, and dryers. The CO₂ stream was compressed and pumped to the dense liquid state at 15 MPa, 25 °C with CO₂ purity of 99.85%. Typical pipeline transport operating conditions ranged approximately between 15 and 30 °C and 10 and 15 MPa [47,48]. The compressor was used from 0.12 MPa to the critical pressure of CO₂, which is 7.38 MPa, and then a pump was used from 7.38 to 15 MPa. For the CO₂ product compression system, the total compression duty was 54.29 MW, and total intercooling duty was 86.73 MW. The CO₂ product pumping power duty was 6.17 MW. Table 3 shows some of the key design and operating conditions of the improved results for the base PCC and compression model integrated with the coal-fired power plant.

Table 3. Key design and operating conditions for improved PCC and compression integrated with Coal and NGCC power plants.

Process Parameter	Unit	Improved Results Coal CO ₂ Capture Plant	Improved Results NGCC CO ₂ Capture Plant
Flue gas flowrate	kg/s	853.1	885.9
Lean solvent flowrate	kg/s	2451	871
L/G ratio	kg/kg	2.87	0.98
Lean solvent CO ₂ loading	mol CO ₂ /mol MEA	0.2082	0.2307
Rich solvent CO ₂ loading	mol CO ₂ /mol MEA	0.5226	0.5000
CO ₂ capture efficiency	%	90	90
Number of absorbers		1	1
Water wash section absorber diameter	m	14.06	13.86
Absorber diameter	m	22.45	18.57
Total absorber packed height	m	41.50	34.50
Number of strippers		1	1
Stripper diameter	m	14.11	8.04
Stripper packed height	m	18	17
Reboiler temperature	°C	117.3	117.1
Regeneration energy requirement	kJ/kgCO ₂	3882	4130
Specific condenser duty	kJ/kgCO ₂	1235	877.82
Blower energy requirement	kJ/kgCO ₂	60	253
Pump energy requirement for Capture plant	kJ/kgCO ₂	13.8	16.98
Compression energy requirement	kJ/kgCO ₂	362	362
Cooling water requirement	kg/s	16320	6489

4.3.2. Improved Results for PCC and Compression with NGCC Power Plant

The improved PCC and compression facility integrated with the NGCC power plant was designed to capture 90% of the CO₂ in the flue gas (FG) from the heat recovery steam generator (HRSG) unit of the power plant. The FG blower was installed upstream of the NGCC power plant DCC to facilitate the effective cooling of the FG before entering the absorber tower. The FG blower operated at an inlet pressure and temperature of 100 kPa and 106 °C, respectively, and an outlet pressure and temperature of 110 kPa and 119.5 °C, respectively, resulting in a blower power duty of 12.8 MW. The DCC cooled and conditioned the FG pressure, temperature, and moisture content so it met the requirement of the absorption column. The temperature and, hence, moisture content of the FG exiting the HRSG was reduced in the DCC, where the FG was cooled using cooling water condensed from the FG and recirculated to the top of the DCC. This slightly affected the condition and compositional amount of the FG that exited the DCC and entered the absorber, resulting in a pressure of 110 kPa, temperature of 40.06 °C, and FG flowrate of 885.9 kg/s.

For the absorption–stripping process, a lean solvent temperature of 40 °C at a pressure of 101.3 kPa and stripper inlet temperature of 110 °C at a pressure of 210 kPa were selected. An optimum solvent flow rate of 871 kg/s, MEA concentration of 30 wt.%, absorber column with Mellapak 250Y packings with a total packed height of 34.50 m, rich CO₂ loading of 0.5000 mol CO₂/mol MEA, stripper column with Mellapak 250Y packings with a total packed height of 17 m, and reboiler temperature of 117.1 °C were obtained with a minimum regeneration energy of 4130 kJ/kgCO₂ at a lean CO₂ loading of 0.2307 mol CO₂/mol MEA.

Optimal parameters of the other ancillary process equipment obtained were as follows: lean/rich heat exchanger duty, 180.67 MW; lean amine cooler duty, 38.99 MW; lean amine pump duty, 136.80 kW; rich amine pump duty, 201.5 kW; water wash section operating temperature, 51 °C; water condenser duty, 108.11 MW; and total cooling water requirement of the NGCC capture plant, 6489 kg/s.

The overhead CO₂ product stream exited from the stripper top at a pressure of 120 kPa, temperature of 93 °C, and CO₂ mass flow of about 182 tons per hour, corresponding to a mass purity of about 97 %. The CO₂ product stream was cooled down to 40 °C in the water condenser, and water was separated from the stream in the water separator. The cooled stream was sent to the five-stage compression system composed of a series of compressors, intercoolers, and dryers. The CO₂ stream was compressed and pumped to the dense liquid state at 15 MPa, 25 °C with CO₂ purity of 99.82%. The compressor was used from 0.12 MPa to the critical pressure of CO₂, which is 7.38 MPa, and then a pump was used from 7.38 to 15 MPa. For the CO₂ product compression system, the total compression duty was 16.49 MW, and total intercooling duty was 26.34 MW. The CO₂ product pumping power duty was 1.87 MW. Table 3 shows some of the key design and operating conditions of the improved results for the base PCC and compression model integrated with the NGCC power plant.

For the same flue gas specifications from the coal and NGCC plants, the design of a double absorber would result in diameter sizes of 17.29 m and 14.70 m for the 550-MWe coal plant and 555-MWe NGCC plant cases, respectively.

4.4. Economic Analysis

The capital cost of the plant (CAPEX) and the operating cost of the plant (OPEX) were calculated for the improved designs for the PCC and compression for both the coal and the NGCC plants. CAPEX is generally assumed to represent the total expenditure required to design, purchase, and install the CO₂ capture plant. OPEX is generally taken to be the operating and maintenance cost required to run and maintain the CO₂ capture plant.

In this study, the CAPEX was taken as the total installed cost needed to acquire the required necessary process equipment and plant facilities, i.e., the capital necessary for the purchase and installation of the process equipment with all components needed for complete process operation, while the OPEX was taken to be the fixed and variable non-fuel operating and maintenance cost required to run and maintain the process plant including labor cost. The levelized cost of electricity

(LCOE), the cost of CO₂ avoided (CAC), and the cost of CO₂ captured were calculated and compared for the process plants. In order to calculate these economic indicators, the total annual cost was computed. The total annual cost is the sum of the total capital cost and operating and maintenance cost. The capital needed to acquire the required necessary process equipment and plant facilities is called the fixed capital cost or investment, while that necessary for the operation of the plant is termed the working capital. The sum of the fixed capital investment and the working capital is known as the total capital investment (TCI). The overall annualized total cost of the capture plant (ATCAPEX) is given by the following equation:

$$ATCAPEX = (CAPEX) \left(\frac{r(1+r)^T}{(1+r)^T - 1} \right) + (OPEX), \quad (15)$$

where r is the interest rate or discount rate, and T is the economic/project life (not including the construction period) of the plant relative to the base year of analysis used in this study.

Table 4 shows the economic evaluation assumptions of the CO₂ capture plant used for the calculation of the ATCAPEX and, hence, the economic indicators.

Table 4. Economic evaluation assumptions.

Parameter	Value
Economic/project life (years)	25
Equipment salvage value (\$)	0
Construction period (years)	3
Capacity factor (%)	85
Interest rate (%)	7
Costs of coal fuel (\$/GJ)	2.37
Costs of NGCC fuel (\$/GJ)	6.85

The calculated characteristic physical sizes of the various equipment in the simulation process flowsheet of the CO₂ capture and compression plant were the basis for estimating the cost of the process equipment.

The base equipment cost estimates of the capture plant were obtained by using the scaling approach utilizing the power relationships of cost capacity concept, given by the following equation [49]:

$$C_a = C_b \left(\frac{index_a}{index_b} \right)^e, \quad (16)$$

where C_a is the estimated cost of the new equipment, C_b is the known cost of given equipment, X is the capacity of new equipment divided by the capacity of given equipment, e is the power factor or cost exponent for specified equipment, $index_a$ is the price index for new equipment, and $index_b$ is the price index for the given or old equipment.

The base size and cost estimates of the equipment cost calculation approach and data outlined by Couper (2012) and Robin (2016) were used for the cost estimations, taking into account the appropriate installation correction factors for materials of construction and operating pressures for specific equipment and all costs adjusted to the common cost year [50,51]. This procedure of estimating the purchased equipment cost depends on the grade of material, the operating conditions, and the size factors representing key characteristics of the equipment. The power exponent factor outlined in Peters et. al. (2004) was used for the calculation of the estimated cost of the new equipment [49]. The estimated capital cost of the compression train and CO₂ product pump model were calculated using the McCollum and Odgen (2006) model [52].

In this study, the composite chemical engineering plant cost index (CEPCI) was used. The composite cost index of 2017 was used to adjust all cost to constant 2017 United States dollars (USD). Hence, all costs are in constant 2017 USD. Table 5 shows the composite CEPCI values used for the calculations. The obtained simulation design physical sizes and operating conditions corresponding to the specified base sizes were used. Table 6 shows the parameters used for the sizing and costing of the CO₂ capture plant equipment to calculate the purchased equipment cost (PEC).

Table 5. Chemical engineering plant cost index (CEPCI).

Year	CEPCI
2000	394.1
2005	468.2
2007	525.4
2009	521.9
2017	567.5

Table 6. Elements used to calculate the purchased cost of the CO₂ capture plant equipment.

Equipment	Size Factor	Base Size	Base Cost (\$)	Power Factor
Blower	Power (kW)	250	98400	0.59
DCC vessel	Weight *			
DCC pump	Power (kW)	4	9840	0.33
DCC cooler	Area (m ²)	80	32,800	0.6
Absorber packed column	Weight *	–	–	–
Stripper packed column	Weight *	–	–	–
Rich pump	Power (kW)	4	9840	0.33
Lean pump	Power (kW)	4	9840	0.33
Lean/rich heat exchanger	Area (m ²)	80	32,800	0.6
Lean cooler	Area (m ²)	80	32,800	0.6
Stripper condenser	Area (m ²)	80	32,800	0.6
Stripper reboiler	Area (m ²)	80	32,800	0.6
Water condenser	Area (m ²)	80	32,800	0.6
Water separator	Weight *	–	–	–

* Cost estimated using direct cost factor from [50].

The costs of the water wash section and other supporting equipment were assumed and taken as percentage addition to the absorber packed column.

The total installed capital cost of the capture plant was calculated based on the purchased equipment cost for each case using the economic parameters of the standardized approach by Chauvel et al. (1981), as shown in Table 7 [53]. This comprises the calculation of the battery limit investment and offsite investment, along with the working capital.

Table 7. Elements to calculate the installed total capital cost of the capture plant. Adapted from [53].

Capital Cost Element	Value
Purchased equipment cost (PEC)	$E_i \forall i = 1, \dots, n$
Instrumentation and controls (ICC)	$I_i \forall i = 1, \dots, n$
Total direct plant cost (DPC)	$\sum_i^n E_i F_E + \sum_i^n I_i F_I$
Indirect plant cost (IPC)	31% DPC
Total direct and indirect plant cost (TDI)	DPC + IPC
Off-sites cost (OC)	31% DPC
Process plant cost (PPC)	TDI + OC
Engineering services (ES)	12% PPC
Royalties paid (RP)	7% TDI
Stationery Items for Office Uses (SIO)	\$338,558 USD in 2017
Facility capital cost (FCC)	PPC + ES + RP + SIO
Solvent/feedstock unit cost (SC)	\$2500/t
Interest on construction (IC)	7% FCC
Start-up cost (SUC)	10% VOM
Total capital cost (TC)	FCC + SC + IC + SUC
Working capital (WC)	10% VOM
Total capital investment (TCI)	TC + WC

F_E , equipment installation factor; F_I , instrument installation factor; VOM , variable operating cost.

After calculating the total capital cost, the operating and maintenance cost was then calculated using the main elements listed in Table 8. The variable cost comprised utilities consumption and amine makeup cost. The fixed cost consisted of maintenance, insurance, labor cost, and overhead cost [53].

Table 8. Elements to calculate fixed and variable operating and maintenance costs of the capture plant [53].

Code	Operating Cost Element	Value
OA	Electricity	\$0.079/kWh
OB	Steam	\$0.018/kWh
OC	Cooling water	\$0.015/m ³
OD	Utilities (U)	$U = OA + OB + OC$
OE	Absorbent makeup	\$2.43/kg
OF	Variable operating cost (VOM)	$VOM = U + OE$
OG	Labor	1 operation engineer (\$/year)
OH	Maintenance	4% PUI
OI	Taxes and insurance	2% PUI
OJ	Overheads	1% PUI
OK	Financing working capital	9% WC
OL	Fixed operating and maintenance (FOM)	$FOM = OG + OH + OI + OJ + OK$

The annualized cost of the CO₂ capture in each case was then calculated from Equation (15). The levelized cost of electricity (LCOE), the cost of CO₂ avoided (CAC), and the cost of CO₂ captured were computed from the following equation:

$$(\text{LCOE})(\$/\text{MWh}) = \frac{(\text{TCR})(\text{FCF}) + (\text{FOM})}{(\text{CF})(8760)(\text{MW})} + \text{VOM} + (\text{HR})(\text{FC}), \quad (17)$$

where TCR is the total capital requirement, FCF is the fixed charge factor (fraction/yr), FOM is the fixed operating and maintenance (O&M) costs (\$/year), VOM is the variable non-fuel O&M costs (\$/MWh), HR is the net power plant heat rate (MJ/MWh), FC is the unit fuel cost (\$/MJ), CF is the plant capacity factor (fraction), 8760 represents the total hours in an typical year, and MW is the net plant capacity (MW).

$$(\text{CAC})(\$/\text{tCO}_2) = \frac{(\text{LCOE})_{\text{CCS}} - (\text{LCOE})_{\text{ref}}}{(\text{tCO}_2/\text{MWh})_{\text{ref}} - (\text{tCO}_2/\text{MWh})_{\text{CCS}}}, \quad (18)$$

where tCO₂/MWh is the CO₂ mass emission rate to the atmosphere in tons per MWh generated, based on the net capacity of each power plant, and the subscripts “ccs” and “ref” refer to plants with and without CCS, respectively.

$$\text{Cost of CO}_2 \text{ Capture}(\$/\text{tCO}_2) = \frac{(\text{LCOE})_{\text{CCS}} - (\text{LCOE})_{\text{ref}}}{(\text{tCO}_2/\text{MWh})_{\text{capture}}}, \quad (19)$$

where tCO₂/MWh captured is the total mass of CO₂ captured in tons per net MWh for the plant with capture. To calculate the overall cost for capture and compression, the characteristic physical sizes of the compression train and CO₂ product pump model developed in this study were implemented in the equations below to compute the capital costs [52].

The compression train capital cost (C_{comp}) was calculated as:

$$C_{\text{comp}} = m_t [(0.13 \times 10^6)(m_t)^{-0.71} + (1.40 \times 10^6)(m_t)^{-0.60} \ln(\frac{P_{\text{Cut-Off}}}{P_{\text{initial}}})], \quad (20)$$

where m_t is the CO₂ mass flow rate through the compression train, P_{initial} is the initial pressure of CO₂ product before compression, and $P_{\text{cut-off}}$ is the critical pressure of CO₂, i.e., 7.38 MPa.

The CO₂ product pump capital cost (C_{pump}) was calculated as

$$C_{\text{pump}} = [(1.11 \times 10^6) \times (\frac{W_p}{1000})] + (0.07 \times 10^6), \quad (21)$$

where W_p is the pumping power requirement, and C_{comp} and C_{pump} are in 2005 \$. Hence, all calculated costs were adjusted to 2017 USD. The annualized costs of the compression train and CO₂ product pump model were computed using the procedure outlined in Table 9.

The overall cost for the CO₂ capture and compression train and CO₂ product pump was calculated by adding the annualized cost of the compression train and CO₂ product pump and the annualized cost of the CO₂ capture plant. The key energy performance and economic analysis results of this study for the coal and NGCC power plants integrated with the CO₂ capture plant and compression models are shown in Tables 10 and 11.

Table 9. Elements to calculate annualized costs of the compression train and CO₂ product pump model.

Cost Element	Value
Capital cost for compression	C _{comp}
Capital cost for CO ₂ product pumping	C _{pump}
Total capital cost (C _{total}) (\$)	C _{comp} + C _{pump}
Capital recovery factor (CRF)	0.15/year
Capacity factor (CF)	0.85
Electricity cost (EC)	\$0.079/kWh
Compression power requirement (W _c)	kW
Pumping power requirement (W _p)	kW
Total compression and pumping power (W _T)	W _c + W _p kW
CO ₂ compressed (mCO ₂)	Tons of CO ₂
CO ₂ compressed per year (CC)	mCO ₂ × CF
Annual capital cost (ACC) (\$)	C _{total} × CRF
Annual operation and maintenance cost (OMC) (\$)	4% C _{total}
Annual electricity power cost (EPC) (\$)	EC × W _T × CF
Total annual cost (C _{annual}) (\$)	ACC + OMC + EPC
Total levelized cost \$/ton CO ₂	(ACC+OMC +EPC) / CC

Table 10. Key energy performance results for the coal and NGCC models.

Case	Coal PCC Model	NGCC PCC Model
Gross power output (kWe)	580,400	564,700
Net power output without capture (kWe)	550,000	555,000
Net power output with capture (kWe)	431,620	507,197
Net power output with capture and compression (kWe)	371,160	488,837
Net plant heat rate with capture (kJ/kWh)	11,669	7847
Power output losses per unit of CO ₂ captured (kW/kgCO ₂)	0.298	0.363
Efficiency with CO ₂ capture only (%)	30.85	45.88
Efficiency with CO ₂ capture and compression (%)	26.53	44.22
Reference plant CO ₂ mass emission rate without capture (t/MWh)	0.802	0.359
Reference plant CO ₂ mass emission rate with capture (t/MWh)	0.165	0.039
Capture plant CO ₂ mass captured rate (t/MWh)	1.392	0.360

For a constant thermal input Q_{th} (Q_{th} = 1,400,162 kW_{th} for coal and Q_{th} = 1,105,812 kW_{th} for NGCC) to the power plants considered in this study, the energy performance results indicate a net efficiency penalty of 12.8% for the coal case and of 6% for the NGCC case when integrated with the PCC and compression model. This resulted in a much lower energy power output for the coal (371,160 kWe) than the NGCC (488,837 kWe) case with both plants having almost the same capacity. However, despite the comparatively lower efficiency penalty for the NGCC case, the specific power output losses per unit of CO₂ captured were lower for coal (0.298 kW/kgCO₂) than for NGCC (0.363 kW/kgCO₂).

Table 11. Results of the economic analysis for the coal and NGCC models.

Cost	Coal PCC Model	NGCC PCC Model
Reference plant LCOE (\$/MWh)	80.69	80.69
Capture plant LCOE ((\$/MWh)	126.71	110.65
Reference plant annual TCI (MM\$)	1364	462
Reference plant TCI (\$/kW)	2480	833
Capture plant annual TCI (MM\$)	347.9	207.9
Total reference plant and capture TCI (\$/kW)	3966	1322
% increase in LCOE of capture over reference plant	57	37
Cost of CO ₂ captured (\$/tCO ₂)	33.55	83.22
Cost of CO ₂ avoided (\$/tCO ₂)	72.25	93.63
Total annual cost of compression (MM\$)	39.86	12.41
Total levelized cost of compression (\$/tCO ₂)	8.67	8.89
Total annual cost of CO ₂ capture and compression (\$/tCO ₂)	400,649.3156	554,883.6833

A comparison of the cost estimates of the coal and NGCC plants with PCC and compression shows that, for the same value of LCOE for both coal and NGCC reference plants, with the addition of capture only, the LCOE increased by up to 37% (from 80.69 to 110.65 \$/MWh) for the NGCC plant and increased by up to 57% (from 80.69 to 126.71 \$/MWh) for the coal plant. However, the levelized cost of electricity per ton of CO₂ compressed of the compression model for both plants was almost the same (7.74 \$/tCO₂). The figures show that the LCOE for the coal plant was more expensive than that for the NGCC plant with capture. However, the escalating higher fuel prices of natural gas for NGCC than coal for coal power plants on the market will make operating the NGCC more cost-competitive than coal plants in terms of LCOE. Figure 14 shows the different variable contributions to the LCOE for both coal and NGCC plants with and without capture. As obtained in this study, the LCOE for the plants was highly sensitive to natural gas prices compared to coal.

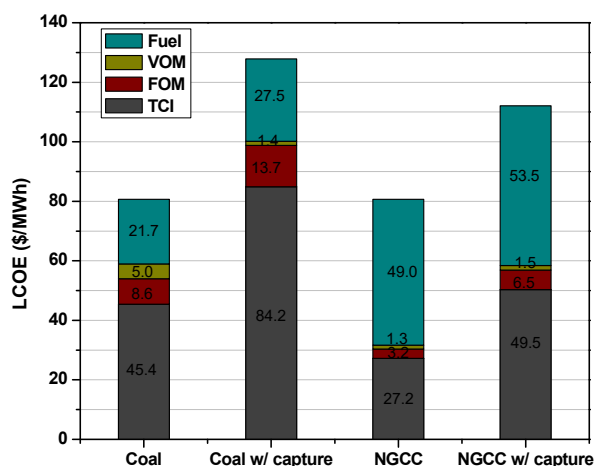


Figure 14. Variable contributions to the LCOE for both coal and NGCC plants. (Fuel = cost of coal or natural gas, VOM = variable non-fuel operating and maintenance (O&M) costs, FOM = fixed operating and maintenance (O&M) costs, TCI = total capital investment).

The cost estimates further show that the cost of CO₂ avoided was lower for coal (72 \$/tCO₂) than for NGCC (94 \$/tCO₂). This indicates that, for the LCOEs of the given power plants without and

with capture to be equal, for the coal and NGCC plant cases, the average CO₂ price should be about 72 \$/tCO₂ for coal and 94 \$/tCO₂ for NGCC, which is about 1.3 times that of coal.

5. Conclusions

In this paper, an energy and economic assessment of an MEA-based post-combustion CO₂ absorption–desorption capture (PCC) and compression system based on optimal design data for coal-fired and natural gas-fired power plants was conducted. The design data of the PCC and compression plants were presented and were obtained using a systematic parametric process design approach. The main aim of the study was an attainment of 90% CO₂ capture rate at a minimum solvent regeneration thermal energy demand for the coal and NGCC PCC and compression plants, as well as to determine their costs. Several vital conclusions can be made from the results obtained for both the coal and the NGCC PCC and compression process. Key amongst them include the following:

1. The recovery percentage of the solute CO₂ in the flue gas mixture and the required product purity of separation were largely determined using the liquid-to-gas molar flow rate (L/G) ratio and the packed height of the absorber or stripper columns. The optimal L/G ratio and reboiler temperature are highly dependent on the lean loading attained and, therefore, determine the regeneration energy. Lower lean loadings enhance the rate behavior of the absorber which increases the capture rate and, hence, increases the solvent regeneration energy. The optimum L/G ratio and CO₂ lean loading for the supercritical pulverized coal PCC plant, with 13.5 mol.% CO₂ in the inlet flue gas, were 2.87 (lean flowrate of 2451 kg/s) and 0.2082 mol CO₂/mol MEA, respectively, while the optimum L/G ratio and CO₂ lean loading for the natural gas combined cycle PCC plant with 4.04 mol.% CO₂ in the inlet flue gas were 0.98 (lean flowrate of 871 kg/s) and 0.2307 mol CO₂/mol MEA, respectively.
2. The above cost estimates indicate that coal plants with capture seem to be the cheapest option for CO₂ capture compared to NGCC plants with capture. Moreover, the study shows that, for the NGCC plant without capture to be cost-competitive with coal plant with capture, the CO₂ price should be 72 \$/tCO₂. The total annual cost of the CO₂ capture and compression plant was lower for Coal (about 400,649 \$/tCO₂) than for NGCC (about 554,884 \$/tCO₂). The decision to invest in NGCC plants with the currently most mature CO₂ capture technology (post-combustion capture and a compression process of the CO₂ for export) largely depends on the prevailing fuel and CO₂ allowance prices on the market.

6. Highlights of Paper

1. A predictive process modeling was used to optimally design post-combustion CO₂ capture and compression plants (PCC) that can be coupled with supercritical pulverized coal-fired and natural gas combined cycle power plants of almost the same capacity.
2. A parametric design approach was used for the design of both plants, and a systematic description of the technical processes for the selection of optimal parameters was presented.
3. A comparative assessment of the energy performance and economic value potential of both plants was presented.

Author Contributions: Supervision, Y.D.Z. and P.T.; Writing—original draft, E.A.; Writing—review and editing, D.L. All authors have read and agreed to the published version of the manuscript.

Funding: The authors acknowledge the financial support of the National Natural Science Foundation of China (51974033), the National Overseas Study Foundation of China (201708420106), the Science and Technology Innovation Foundation of PetroChina (No. 2015D-5006-0603), and the Yangtze Youth Talents Fund (No. 2015cqt01).

Conflicts of Interest: The authors declare no conflict of interest.

References

1. Szulejko, J.E.; Kumar, P.; Deep, A.; Kim, K.-H. Global warming projections to 2100 using simple CO₂ greenhouse gas modeling and comments on CO₂ climate sensitivity factor. *Atmos. Pollut. Res.* **2017**, *8*, 136. [CrossRef]
2. Pillar-Little, E.A.; Guzman, M.I. An Overview of Dynamic Heterogeneous Oxidations in the Troposphere. *Environments* **2018**, *5*, 104. [CrossRef]
3. PBL Netherlands Environmental Assessment Agency. *Trends in Global CO₂ Emissions; 2016 Report*; Netherlands Environmental Assessment Agency: Rijswijk, The Netherlands, 2016.
4. USEPA, "Greenhouse Gas Emissions", United States Environmental Protection Agency. 2017. Available online: <https://www.epa.gov/ghgemissions/global-greenhouse-gas-emissions-data> (accessed on 6 November 2017).
5. Steeneveldt, R.; Berger, B.; Torp, T. CO₂ capture and storage. *Chem. Eng. Res. Des.* **2006**, *84*, 739–763. [CrossRef]
6. Kuramochi, T.; Ramírez, A.; Turkenburg, W.; Faaij, A. Comparative assessment of CO₂ capture technologies for carbon-intensive industrial processes. *Prog. Energy Combust. Sci.* **2012**, *38*, 87–112. [CrossRef]
7. Abas, N.; Kalair, A.; Khan, N. Review of Fossil Fuels and Future Energy Technologies. *Futures* **2015**. [CrossRef]
8. WCA, Coal and Electricity, World Coal Association. 2018. Available online: <https://www.worldcoal.org/coal/uses-coal/coal-electricity> (accessed on 25 April 2018).
9. Huaman, R.N.E.; Jun, T.X. Energy Related CO₂ Emissions and the Progress on CCS Projects: A review. *Renew. Sustain. Energy Rev.* **2014**, *31*, 368–385. [CrossRef]
10. Leung, D.Y.C.; Caramanna, G.; Maroto-Valer, M.M. An Overview of Current Status of Carbon Dioxide Capture and Storage Technologies. *Renew. Sustain. Energy Rev.* **2014**, *39*, 426–443. [CrossRef]
11. Zhou, R.; Guzman M., I. CO₂ Reduction under Periodic Illumination of ZnS. *The J. Phy. Chem.* **2014**, *118*.
12. Sharma, N.; Das, T.; Kumar, S.; Bhosale, R.; Kabir, M.; Ogale, S. Photocatalytic Activation and Reduction of CO₂ to CH₄ over Single Phase Nano Cu₃SnS₄: A Combined Experimental and Theoretical Study. *ACS Appl. Energy Mater.* **2019**, *2*, 5677–5685. [CrossRef]
13. IEA. *Carbon Capture and Storage, the Solution for Deep Emissions Reductions*; OECD/IEA Publishing: Paris, France, 2015.
14. Liang, Z.H.; Rongwong, W.; Liu, H.; Fu, K.; Gao, H.; Cao, F.; Zhang, R.; Sema, T.; Henni, A.; Sumon, K.; et al. Recent progress and new developments in post-combustion carbon-capture technology with amine-based solvents. *Int. J. Greenh. Gas Control.* **2015**, *40*, 26–54. [CrossRef]
15. IEA Report, Energy Technology Perspectives. 2010. Available online: <http://www.iea.org> (accessed on 9 May 2019).
16. GCCSI. *The Global Status of CCS; Summary Report 2019*; Global CCS Institute (GCCSI): Melbourne, Australia, 2019.
17. Rubin, E. 2012 Understanding the Pitfalls of CCS Cost Estimates. *Int. J. Greenh. Gas Control* **2012**, *10*, 181–190. [CrossRef]
18. Idem, R.; Wilson, M.; Tontiwachwuthikul, P.; Chakma, A.; Veawab, A.; Aroonwilas, A.; Gelowitz, D. Pilot plant studies of the CO₂ capture performance of aqueous MEA and mixed MEA/MDEA solvents at the University of Regina CO₂ capture technology development plant and the Boundary Dam CO₂ capture demonstration plant. *Ind. Eng. Chem. Res.* **2006**, *45*, 2414–2420. [CrossRef]
19. Notz, R.; Mangalapally, H.P.; Hasse, H. Post combustion CO₂ capture by reactive absorption: Pilot plant description and results of systematic studies with MEA. *Int. J. Greenh. Gas Control* **2012**, *6*, 84–112. [CrossRef]
20. Frimpong, R.A.; Johnson, D.; Richburg, L.; Hogston, B.; Remias, J.E.; Neathery, J.K.; Liu, K. Comparison of solvent performance for CO₂ capture from coal-derived flue gas: A pilot scale study. *Chem. Eng. Res. Des.* **2013**, *91*, 963–969. [CrossRef]
21. Thompson, J.G.; Combs, M.; Abad, K.; Bhatnagar, S.; Pelgen, J.; Beaudry, M.; Rochelle, G.; Hume, S.; Link, D.; Figueroa, J.; et al. Pilot testing of a heat integrated 0.7 MWe CO₂ capture system with two-stage air-stripping: Emission. *Int. J. Greenh. Gas Control* **2017**, *64*, 267–275. [CrossRef]
22. Thompson, J.G.; Bhatnagar, S.; Combs, M.; Abad, K.; Onneweer, F.; Pelgen, J.; Link, D.; Figueroa, J.; Nikolic, H.; Liu, K. Pilot testing of a heat integrated 0.7 MWe CO₂ capture system with two-stage air-stripping: Amine degradation and metal accumulation. *Int. J. Greenh. Gas Control* **2017**, *64*, 23–33. [CrossRef]

23. Berstad, D.; Arasto, A.; Jordal, K.; Haugen, G. Parametric study and benchmarking of NGCC, coal and biomass power cycles integrated with MEA-based post-combustion CO₂ capture. *Energy Procedia* **2011**, *4*, 1737–1744. [[CrossRef](#)]
24. Mac Dowell, N.; Shah, N. Dynamic modelling and analysis of a coal-fired power plant integrated with a novel split-flow configuration post-combustion CO₂ capture process. *Int. J. Greenh. Gas Control* **2014**, *27*, 103–119. [[CrossRef](#)]
25. Ali, U.; Font-Palma, C.; Akram, M.; Agbonghae, E.O.; Ingham, D.B.; Pourkashanian, M. Comparative potential of natural gas, coal and biomass fired power plant with post—Combustion CO₂ capture and compression. *Int. J. Greenh. Gas Control* **2017**, *63*, 184–193. [[CrossRef](#)]
26. Freguia, S.; Rochelle, G.T. Modeling of CO₂ capture by aqueous monoethanolamine. *AIChE J.* **2003**, *49*, 1676–1686. [[CrossRef](#)]
27. Zhang, Y.; Chen, H.; Chen, C.C.; Plaza, J.M.; Dugas, R.; Rochelle, G.T. Rate-based process modeling study of CO₂ capture with aqueous monoethanolamine solution. *Ind. Eng. Chem. Res.* **2009**, *48*, 9233–9246. [[CrossRef](#)]
28. Chen, C.-C.; Britt, H.I.; Boston, J.F.; Evans, L.B. Local composition model for excess Gibbs energy of electrolyte systems. Part I: Single solvent, single completely dissociated electrolyte systems. *AIChE J.* **1982**, *28*, 588–596. [[CrossRef](#)]
29. Chen, C.C.; Evans, L.B. A Local Composition Model for the Excess Gibbs Energy of Aqueous-Electrolyte Systems. *AIChE J.* **1986**, *32*, 444–454. [[CrossRef](#)]
30. Peng, D.-Y.; Robinson, D.B. A New Two-Constant Equation of State. *Ind. Eng. Chem. Fundam.* **1976**, *15*, 59–64. [[CrossRef](#)]
31. Hessen, E.T.; Haug-Warberg, T.; Svendsen, H.F. The refined e-NRTL model applied to CO₂–H₂O–alkanolamine systems. *Chem. Eng. Sci.* **2010**, *65*, 3638–3648. [[CrossRef](#)]
32. Wilcox, J. *Carbon Capture*; Springer Science+Business Media, LLC: New York, NY, USA, 2012.
33. USDOE/NETL. *Cost and Performance Baseline for Fossil Energy Plants, Volume 1: Bituminous Coal and Natural Gas to Electricity*; Revision 2a, September 2013, DOE/NETL- 2010/1397; US Department of Energy/National Energy Technology Laboratory: Washington, DC, USA, 2010 20 September; 13.
34. Shen, K.-P.; Li, M.-H. Solubility of Carbon Dioxide in Aqueous Mixtures of Monoethanolamine with Methyl-diethanolamine. *J. Chem. Eng. Data* **1992**, *37*, 96–100. [[CrossRef](#)]
35. Cifre, P.G.; Brechtel, K.; Unterberger, S.; Scheffknecht, G. Experimental studies on CO₂ desorption from amine solutions. In Proceedings of the IEA 4th International Conference of Clean Coal Technologies, Dresden, Germany, 18–20 May 2009.
36. Oexmann, J.; Kather, A. Minimising the regeneration heat duty of post-combustion CO₂ capture by wet chemical absorption: The misguided focus on low heat of absorption solvents. *Int. J. Greenh. Gas Control* **2010**, *4*, 36–43. [[CrossRef](#)]
37. Sander, M.T.; Mariz, C.L. The Fluor Daniel® econamine FG process: Past experience and present day focus. *Energy Convers. Manag.* **1992**, *33*, 341–348. [[CrossRef](#)]
38. Kohl, A.L.; Nielsen, R.B. *Gas Purification*, 5th ed.; Gulf Professional Publishing: Houston, TX, USA, 1997.
39. Fenske, M.R. Fractionation of Straight-Run Pennsylvania Gasoline. *Ind. Eng. Chem.* **1932**, *24*, 482. [[CrossRef](#)]
40. Underwood, A.J.V. Fractional Distillation of Multicomponent Mixtures. *Chem. Eng. Prog.* **1948**, *1948* *44*, 603. [[CrossRef](#)]
41. Gilliland, E.R. Multicomponent Rectification. *Ind. Eng. Chem.* **1940**, *32*, 1220. [[CrossRef](#)]
42. Davis, J.; Rochelle, G. Thermal degradation of monoethanolamine at stripper conditions. In Proceedings of the 9th International Conference on Greenhouse Gas Control Technologies, Washington, DC, USA, 16–20 November 2008.
43. Li, X.; Wang, S.; Chen, C. Experimental study of energy requirement of CO₂ desorption from rich solvent. *Energy Procedia* **2013**, *37*, 1836–1843. [[CrossRef](#)]
44. Canepa, R.; Wang, M. Techno-economic analysis of a CO₂ capture plant integrated with a commercial scale combined cycle gas turbine (CCGT) power plant. *Appl. Therm. Eng.* **2014**. [[CrossRef](#)]
45. Alhajaj, A.; Mac Dowell, N.; Shah, N. A techno-economic analysis of post-combustion CO₂ capture and compression applied to a combined cycle gas turbine: Part I. A parametric study of the key technical performance indicators. *Int. J. Greenh. Gas Control* **2016**, *44*, 26–41. [[CrossRef](#)]
46. Vaidya, P.D.; Kenig, E.Y. CO₂-alkanolamine reaction kinetics: A review of recent studies. *Chem. Eng. Technol.* **2007**, *30*, 1467–1474. [[CrossRef](#)]

47. Wang, D.; Zhang, Y.D.; Adu, E. Influence of Dense Phase CO₂ Pipeline Transportation Parameters. *Int. J. Heat Technol.* **2016**, *34*, 479–484. [[CrossRef](#)]
48. Adu, E.; Zhang, Y.D.; Liu, D. Current Situation of Carbon Dioxide Capture, Storage, and Enhanced Oil Recovery in the Oil and Gas Industry. *Can. J. Chem. Eng.* **2019**, *97*, 1048–1076. [[CrossRef](#)]
49. Peters, M.S.; Timmerhaus, K.D.; West, R.E. *Plant Design and Economics for Chemical Engineers*, 5th ed.; McGraw Hill: New York, NY, USA, 2004.
50. Couper, J.R.; Penney, W.R.; Fair, J.R.; Walas, S.M. *Chemical Process Equipment: Selection and Design*, 3rd ed.; Elsevier Butterworth-Heinemann: Amsterdam, The Netherlands; London, UK, 2012.
51. Robin, S. *Chemical Process Design and Integration*, 2nd ed.; John Wiley & Sons Ltd.: Chichester, UK, 2016.
52. McCollum, D.L.; Ogden, J.M. *Techno-Economic Models for Carbon Dioxide Compression, Transport, and Storage & Correlations for Estimating Carbon Dioxide Density and Viscosity*; Institute of Transportation Studies, University of California: Davis, CA, USA, 2006.
53. Chauvel, A.; Miller, R.; Miller, E.B. *Manual of Economic Analysis of Chemical Processes: Feasibility Studies in Refinery and Petrochemical Processes*; McGraw-Hill: New York, NY, USA, 1981.



© 2020 by the authors. Licensee MDPI, Basel, Switzerland. This article is an open access article distributed under the terms and conditions of the Creative Commons Attribution (CC BY) license (<http://creativecommons.org/licenses/by/4.0/>).